

Accepted Manuscript

Title: Ultrasonic-Assisted Green Synthesis of β -Amino Carbonyl Compounds by Copper Oxide Nanoparticles Decorated Phosphate Functionalized Graphene Oxide via Mannich Reaction

Authors: L. Satish K. Achary, Pratap S. Nayak, Bapun Barik, Aniket Kumar, Priyabrat Dash



PII: S0920-5861(19)30406-7
DOI: <https://doi.org/10.1016/j.cattod.2019.07.050>
Reference: CATTOD 12379

To appear in: *Catalysis Today*

Received date: 19 May 2019
Revised date: 27 July 2019
Accepted date: 29 July 2019

Please cite this article as: Achary LSK, Nayak PS, Barik B, Kumar A, Dash P, Ultrasonic-Assisted Green Synthesis of β -Amino Carbonyl Compounds by Copper Oxide Nanoparticles Decorated Phosphate Functionalized Graphene Oxide via Mannich Reaction, *Catalysis Today* (2019), <https://doi.org/10.1016/j.cattod.2019.07.050>

This is a PDF file of an unedited manuscript that has been accepted for publication. As a service to our customers we are providing this early version of the manuscript. The manuscript will undergo copyediting, typesetting, and review of the resulting proof before it is published in its final form. Please note that during the production process errors may be discovered which could affect the content, and all legal disclaimers that apply to the journal pertain.

Ultrasonic-Assisted Green Synthesis of β -Amino Carbonyl Compounds by Copper Oxide Nanoparticles Decorated Phosphate Functionalized Graphene Oxide via Mannich Reaction

L. Satish K. Achary^a, Pratap S. Nayak^a, Bapun Barik^a, Aniket Kumar^b and Priyabrat Dash^{*a}

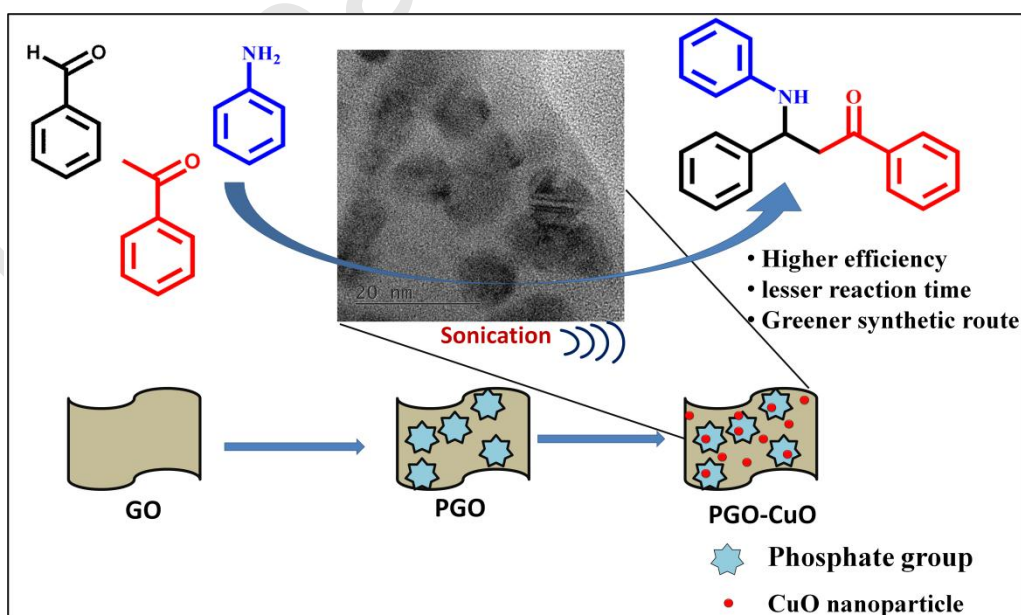
^aDepartment of Chemistry, National Institute of Technology, Rourkela, Orissa, 769008,

^bSchool of Materials Science and Engineering, Chonnam National University, Gwang-Ju, 61186, Republic of Korea.

Email id (corresponding author): dashp@nitrkl.ac.in

Graphical Abstract

Highly efficient and active CuO nanoparticle decorated Phosphate functionalised graphene oxide (PGO-CuO) nanocomposite has been synthesized in a water-isopropanol system and used as an active catalyst for the synthesis of β -amino carbonyl compounds via Mannich reaction by using a greener ultrasonic method.



Highlights

- CuO nanoparticles were decorated on PGO via a simple wet chemical synthetic route.
- PGO-CuO catalyst was thoroughly characterized by various analytical techniques.
- A greener ultrasonic route was used for synthesis of β -amino carbonyl compounds.
- Higher catalytic efficiency was obtained under solventless condition.
- The catalyst could be recycled for six times without any effective loss in activity.

Abstract

A facile chemical synthetic route has been demonstrated for the synthesis of copper oxide nanoparticles decorated phosphate functionalized graphene oxide (*CuO/PGO*). The synthesized nanocatalyst was used as an efficient and active candidate for the synthesis of β -amino carbonyl compounds via a green synthetic ultrasonic route. The structural properties of the samples were investigated by means of a number of sophisticated techniques like X-ray diffraction (XRD), Fourier-transform Infrared (FTIR) spectroscopy, High Resolution Transmission Electron Microscope (HRTEM), N₂ adsorption-desorption measurements, X-ray photoelectron spectroscopy (XPS) analysis, Ammonia temperature programmed desorption analysis (NH₃-TPD) and Raman spectroscopy. HRTEM analysis confirmed the presence of spherical CuO nanoparticles distributed uniformly throughout the PGO surface. XPS analysis demonstrated the presence of Cu²⁺ species and minor reduction of oxygen functional groups on GO. A higher surface area of 162 m²/g for *CuO/PGO* was found from N₂ adsorption-desorption isotherms. Later on, the presence of acidic groups on *CuO/PGO* that play an essential role in the catalytic activity was examined by NH₃-TPD and pyridine adsorbed IR analysis. The total acidity on the surface of

synthesized nanocatalyst was found to be of 0.59 mmol g^{-1} which includes both Lewis as well as Brönsted acidic sites. A higher product yield of 95% in a shorter period of time of 15 min was achieved which is superior to many reported catalytic systems. A combined strategy involving greener and easier ultrasonic route and use of an efficient acidic graphene oxide-based catalyst resulted in higher catalytic activity and stability with with good recyclability.

Keywords: Ultrasonic assisted, β -amino carbonyl compounds, phosphate functionalized graphene oxide and CuO nanoparticles.

1. Introduction

Acid catalysis has become an important pathway for the synthesis of many important industrial chemicals [1]. A wide range inorganic/organic acids and stoichiometric amounts of acidic sites are normally used for various industrial reactions. Friedel–Crafts alkylations, nitrations, aromatic halogenations, acylations, condensation and oligomerisations are some of the well known acid catalyzed reactions [2-5]. Most commonly used catalysts for these reactions are Brönsted acids like H_2SO_4 , HCl , HClO_4 and HF and Lewis acids like BF_3 , AlCl_3 and $\text{ZnO-Al}_2\text{O}_3$ [6-8]. However, the use of these acids have a number of drawbacks such as hazardous in handling, corrosiveness, lack of reusability and production of large volume of toxic and corrosive wastes. These drawbacks facilitated researchers to design suitable alternative catalysts. In this regard, solid acid materials are found to be promising material in which various support materials are normally used for the design of such catalysts. Owing to the unique properties of carbon-based materials like graphene and carbon nanotubes (CNT), various acid groups that can act as active sites have been incorporated on their surface inorder to design active and efficient nanocatalyst. For example, Xiao and co-workers reported sulfonated graphene as an enhanced solid nanocatalyst for acid catalyzed esterification reaction [9]. In another work, Yue *et al.* showcased the enhanced catalytic properties of aminoacid functionalised multiwalled carbon nanotubes

towards asymmetric reduction of aromatic ketones [10]. In all the cases, carbon-based materials have shown promising support material for acid catalyzed reactions.

Among other carbon-based materials, graphene oxide (GO) has become an important support material as it has unique structural and physicochemical properties [11-13]. Especially in the field of catalysis, GO has been used as a best support material due to its unique structural properties like high specific surface area and easy surface modification [14]. The modification of its surface becomes facile because of the presence of hydrophilic oxygen functional groups including carbonyl, carboxylic group, epoxide and hydroxyl groups. This helps for the immobilization of the active species which are responsible for catalysis [15]. In this regard, various acidic groups such as phosphate and sulfonate functional group have been used for the modification of graphene oxide surface [16-18]. In particular, phosphate groups would be an suitable candidate to design an efficient solid nanocatalyst as it provides several advantages such as high charge carrier concentration, thermal stability, oxidation resistance and possible proton conduction in the dry state by forming dynamic hydrogen bond networks [19]. Therefore, more studies are required to study the suitability of phosphate functionalized GO (PGO) catalyst for various catalytic reactions.

Over the past few years, there is a considerable interest in the development of nitrogen-based heterocycles due to their diverse activities. Among these heterocycles, β -amino carbonyl compounds are found to be an important and essential type of nitrogen-based heterocyclic compound which attracts most of the pharmaceutical industry because of their interesting biological activities such as antitumor, antibacterial, anticancer, and anti-inflammatory activity [20, 21]. They also act as fundamental building blocks for the preparation of important molecules like amino alcohols, peptides, lactams and as precursors to synthesize amino acids. [22]. Also, these compounds are regarded as important synthetic intermediate for various natural products like alkaloids and polyketides [23]. The most preferable path

for the synthesis of these β -amino carbonyl compounds is Mannich reaction which involves a three component condensation of aldehyde, ketone and amine. Many acidic groups (sulfonic acid and heteropolyacids) as well as metal/metal oxide nanoparticles (sulfated alumina and zirconia) have been reported as efficient catalyst for this type of reaction [24-30]. However, these catalysts have various drawbacks like more time consumption for reaction, inadequate yields, non-greener method and use of expensive catalyst. Moreover the methodologies used for the synthesis have drawbacks such as longer reaction time and high power consumption. As both acids as well as metal oxide nanoparticles were successfully used for synthesis of β -amino carbonyl compounds we envisioned that by modifying metal oxide nanoparticles on acidic GO (PGO) surface would potentially make a novel nanocatalyst for this type of Mannich reaction. In this regards, CuO nanoparticle modified PGO would be a potential nanocatalyst for such reaction as CuO nanoparticle have high surface area, good chemical and thermal stability and reactive morphologies [31]. It also provides several other advantages like low cost, ease of handling and good reusability. To the best of our knowledge, such system have earlier not been reported.

With an aim to design a novel and highly efficient heterogeneous nanocatalyst for synthesis of β -amino carbonyl compounds via greener route, herein, we report an ultrasonic assisted methodology using CuO decorated PGO (*CuO/PGO*) as potential catalyst. Ultrasonic assisted methodology was chosen as it generates high temperatures and pressures in a very short period of time (about 10-15 sec) making this as a more efficient and greener route for organic syntheses. The β -amino carbonyl compounds were synthesized via condensation of benzaldehyde, acetophenone and aniline in the presence of our designed nanocatalyst (*CuO/PGO*) as shown in scheme1 and the same reaction pathway was applied for the synthesis of other derivatives. The designed nanocatalyst was highly active towards all the reactions within a shorter period of time as compared to other traditionally available catalysts with less

consumption of energy. Moreover, our catalyst was highly stable after six reaction cycles with minimal loss in activity.

2. Experiment

2.1. Materials and instrumentation

Graphite powder, triethylphosphite, CDCl_3 , $\text{Cu}(\text{OAc})_2 \cdot \text{H}_2\text{O}$ and LiBr were purchased from Sigma-Aldrich. H_2O_2 (30%), NaNO_3 , ethanol, HCl , KMnO_4 , silica gel (100-200 mesh) and H_2SO_4 were purchased from Hi-Media. 18 M Ω cm Milli-Q water was used throughout the syntheses. All the chemicals were used without any further purification. X-ray diffraction study of the catalyst was done by using Philips PW 1830 X-ray diffractometer with $\text{Cu K}\alpha$ source (1.54 \AA). Perkin-Elmer FTIR spectrophotometer was used to record the FTIR spectra of the catalyst using NaCl support. Philips CM 200 equipment was used for the transmission electron microscopy (TEM) analysis of the synthesized sample using carbon coated nickel grids. The Raman analysis was recorded using Bruker RFS 27 spectrometer with 1064 nm wavelength incident laser light. Surface area analysis was done by nitrogen adsorption/desorption analysis using a Quantachrome Autosorb 3-B apparatus. ^1H NMR and ^{13}C NMR spectra were recorded using Bruker spectrometer at 400 MHz using TMS as an internal standard. A Multi Lab 2000 (Thermo VG Scientific, United Kingdom) was used to record the XPS spectra. Micromeritics Chemisorb 2750 TPD unit was used for the NH_3 -TPD analysis of the catalyst. *Ultrasonic syntheses were carried out in an ultrasonic cleaning bath GT Sonic-L3, (multi-frequency at 45 and 65 kHz).* The progress of catalytic reaction was monitored by using thin layer chromatography (TLC) on 0.2 mm silica gel F-254 plates. All the pure products obtained were identified by comparing their spectral characteristics with the literature reported values.

2.2. Catalyst preparation

2.2.1. Synthesis of *CuO/PGO* nanocatalyst

GO was synthesized via modified Hummers' method using natural graphite flake [32]. Then PGO was synthesized via Arbuzov reaction [33]. Later on, PGO was decorated with CuO nanoparticles to prepare *CuO/PGO* nanocatalyst in water-isopropyl system (scheme 1) [34]. Briefly, 200 mg of PGO was taken along with 50 ml of isopropyl alcohol and ultrasonicated for 30 min to afford a black dispersion. Under continuous ultrasonic irradiation, 0.14 g of $\text{Cu}(\text{OAc})_2 \cdot \text{H}_2\text{O}$ was added to the homogeneous dispersion resulting in the formation of brown colored solution. Then it was heated at 85 °C under continuous stirring for 30 min. After that 20 mL of deionized (DI) water was added rapidly into the above dispersion and allowed it for further heating at 85 °C for 30 min. The colour of the dispersion gradually changed to black. *In the next step, the reaction mixture was cooled and centrifuged. Then the solid product was washed with ethanol several times and dried at 70 °C in air overnight without any calcination process. Our primary aim was to design a highly active solid nanocatalyst for synthesis of β -amino carbonyl compounds. Calcination of the catalyst under high temperature may reduce the active acidic sites present on the catalyst. Hydrolysis in water-isopronol system with multiple washing in ethanol resulted in the removal of unreacted $\text{Cu}(\text{OAc})_2 \cdot \text{H}_2\text{O}$.*

2.3. Synthesis of 3-Anilino-1,3-diphenyl-1-propanone

2.3.1. Traditional method

In brief, aniline (1 mmol), benzaldehyde (1 mmol) and acetophenone (1 mmol) were taken in a round bottom flask and mixed thoroughly. *CuO/PGO* (0.03 g) catalyst was added to the resulting mixture and then stirred at 40 °C for 20 min without any solvent. During this process, the reaction progress was monitored by thin layer chromatography (TLC). Finally, the solid crude was recovered and washed with distilled water and 20ml of ethyl acetate. In this process, the unreacted organic part was removed and the solid crude was dissolved. The mixture was sonicated for 2-3 min and the solid catalyst was separated

by centrifugation and dried at 90 °C in oven. The desired product was separated and purified by column chromatography.

2.3.2. ultrasonic assisted method

In brief, aniline (1 mmol), benzaldehyde (1 mmol) and acetophenone (1 mmol) were taken along with 0.03 g of catalyst (*CuO/PGO*). Then, the glass vial was placed in the bath sonicator to interact with ultrasonic wave. By TLC, the reaction progress was monitored. The time period of the ultrasonic wave irradiation was for 15-20 min. After the completion of reaction, the resulting crude was dissolved in ethanol and the solid catalyst was recovered by centrifugation. The solid catalyst was thoroughly washed with ethanol and then separated from the reaction mixture. Then it was dried under vacuum and reused. The final product was purified by column and all the products were characterized by comparison of their spectral data with those for authentic samples.

3. Results and discussion

3.1. Characterization of *CuO/PGO* catalyst

During Hummers' method various hydrophilic oxygen functional groups are generated on GO surface which make it an eligible candidate for support material in catalysis. Moreover, the introduction of acidic groups on GO surface generate more active centers which further enhance its catalytic activity. Envisioning the above possibility, we have employed Arbuzov reaction for the synthesis of phosphate functionalized GO and used a simple water-isopropanol system to incorporate the CuO nanoparticles. We expected that the introduction of metal oxide nanoparticles in the functionalised GO would further increase the active sites. The resulting solid acid *CuO/PGO* catalyst was then thoroughly characterised by different sophisticated analytical techniques such as PXRD, FTIR, TEM analysis, N₂ adsorption desorption, XPS, NH₃-TPD and Pyridine adsorbed IR.

Initially, the structural investigation was carried out with XRD and FTIR to confirm the crystallinity and phase purity as well as the presence of essential functional groups on the surface of *CuO/PGO* (Fig.1). From the XRD spectra of GO, a sharp diffraction peak was found at $2\theta = 10.4^\circ$ which is normally appeared for (002) planes of GO due to the presence of the uniform graphitic layer. After functionalization with the phosphate group, the sharp (002) peak vanished which suggested exfoliation of individual graphene layers by the incorporation of the phosphate groups. The presence of a poor crystalline nature of functionalized GO was indicated due to a broad peak at around $2\theta = 22^\circ$. This indicated that the sheets are randomly oriented and fully exfoliated by the incorporation of the phosphate groups. After the decoration of CuO nanoparticles, some sharp peaks have been seen in the XRD spectra of *CuO/PGO* nanocatalyst confirming the crystalline nature of the nanocatalyst. All the diffraction peaks appeared in XRD pattern confirmed the presence of CuO lattice which are with good agreement with JCPDS: 80-1268 file. Overall, the purity and crystalline nature of the *CuO/PGO* nanocatalyst was inferred by the above results. Similar XRD pattern for CuO nanoparticles can also be found in other literature [35].

To further check the purity of the material and the functional groups present on its surface, FTIR analysis was carried out. FTIR spectrum of GO, PGO as well as the *CuO/PGO* nanocatalyst are shown in Fig. 1 (b). The FTIR spectra of GO shows the absorption peaks at 1052, 3410 and 1724 cm^{-1} suggesting the presence of C-O-C, -OH and C=O in carboxylic acid groups respectively. After functionalization of phosphate groups, new absorption peaks at 600, 960 and 1020 cm^{-1} appeared which can be attributed to different vibrational mode of phosphate group [36]. These peaks can also be seen in the FTIR spectra of desired nanocatalyst (*CuO/PGO*). In addition, some new peaks can be seen at 510 cm^{-1} and 450 cm^{-1} corresponding to Cu-O stretching vibrations [37]. Besides, the absence of two sharp peaks at nearly 1401 and 1630 cm^{-1} corresponding to acetate ion indicated the absence of any

unreacted acetate ion on our catalyst surface. Hydrolysis of acetate salt under high temperature in presence of isopropanol and water solvent resulted in the formation of CuO nanoparticle. Therefore, the possible presence of $\text{Cu}(\text{OAc})_2$ metal precursor in the prepared nanocatalyst (CuO/PGO) can be discarded in this synthesis process. Similar procedures are available in literatures in which CuO nanoparticles have been successfully synthesized in alcohol without calcination [38].

Both the above techniques (XRD & FTIR) confirmed the coexistence of phosphate group and CuO nanoparticle in the CuO/PGO nanocatalyst which are essential for acid catalyzed reaction. *The dimensions (shape) and surface morphology of the designed active solid nanocatalyst (CuO/PGO) were then thoroughly studied via TEM analysis (Fig. 2). The 2-dimensional layered structure of GO was clearly observed in the TEM image on which phosphate groups are successfully incorporated (Fig. 2(a)). The spherical CuO nanoparticles are seen to be uniformly distributed throughout the layer having size range of several nanometers (5–8 nm) as shown in Fig. 2(b). The lattice spacing of the CuO nanoparticle taken from the HRTEM image of an individual nanoparticle is found to be 0.26 nm and can be ascribed to $(\bar{1}11)$ plane of CuO (Fig. 2(c)) [39]. The crystalline nature of the material can be validated from the SAED pattern which shows clear ring structure as seen in Fig. 2(d). The elemental composition of the nanocatalyst was also investigated by EDX spectral analysis. It was confirmed that our nanocatalyst contains elements like C, O, P and Cu. All the above results from the TEM analysis confirmed the successful deposition of CuO nanoparticles on PGO surface and the pattern is in good agreement with the previously reported results [40] [41].*

Development of any surface defects during the synthesis of PGO and after the decoration of CuO nanoparticles was then confirmed by Raman analysis. Raman spectra of GO, PGO and CuO/PGO are shown in Fig. S1. Two distinct peaks can be seen at 1593 and 1362cm^{-1} for GO, which are mainly due to the vibration of sp^2 carbon atoms in a graphitic 2D hexagonal lattice (G band) and the vibrations of sp

carbon atoms of defects and disorder (D band), respectively. The intensity ratio of these two bands (I_D/I_G) has been considered an indicator of the degree of carbon defects. When the Raman spectra of PGO and *CuO/PGO* were compared to the Raman spectra of GO it was found that I_D/I_G value of GO was 0.96 where as for PGO and *CuO/PGO* the value increased to 1.05 and 1.09 respectively. Moreover, in comparison to GO and PGO, the G and D band of *CuO/PGO* nanocatalyst was slightly shifted to 1581 cm^{-1} and 1349 cm^{-1} respectively. This suggested the increased disorderness on the GO surface. These type of observations have been seen from various previously reported studies [42]. It can be concluded that functionalization of phosphate group followed by decoration of CuO nanoparticles on the parent material (GO) generated defect sites which results in the destruction of conjugated carbon lattice.

After surface modification of GO with phosphate groups as well as with CuO nanoparticles, the surface became rough which was seen from the HRTEM image. This change in surface morphology would facilitate an increase in surface area of the final *CuO/PGO* material. Hence, N_2 adsorption-desorption measurements were carried out and the results are shown in Fig. 3. All the isotherms were formed to be type IV isotherm according to the IUPAC classification [43]. Surface area for GO was found to be $154\text{ m}^2\text{ g}^{-1}$ which increased to $179\text{ m}^2\text{ g}^{-1}$ for PGO due to the reduction of GO surface during functionalization. However, the surface area of *CuO/PGO* was decreased to $163\text{ m}^2\text{ g}^{-1}$. This decrease in surface area is mainly due to the surface covering with CuO nanoparticles. However, the resulting surface area of the designed nanocatalyst is higher than the parent material (GO) which indicated that more reactant molecules would be facilitated for interaction during the catalytic reaction.

X-ray photoelectron spectroscopy (XPS) is a vital and powerful technique to investigate the presence of different chemical environment in an unknown sample [44]. The presence of phosphate groups as well as CuO nanoparticles in *CuO/PGO* nanocatalyst was previously confirmed from FT-IR and TEM analysis. To further confirm the successful synthesis of the desired nanocatalyst (*CuO/PGO*), presence

of different functional groups and oxidation state of Cu, XPS analysis was carried out (Fig. 4). In Fig. 4a, the presence of phosphorus and copper in the nanocatalyst can be confirmed from the new peaks appeared at 132.4 and 935.1 eV which can be attributed to P2p and Cu2p core level spectra, respectively. Minor reduction of oxygen functional groups can be observed from core level XPS spectrum of C1s of CuO/PGO (Fig. 4 (b,c)). This reduction was mainly occurred during the functionalisation of phosphate group on the GO surface, which is the main reason for its higher surface area as compared to GO. The core level XPS spectrum of Cu2p shown in Fig. 4 (e) has two distinct peaks (doublet) at 934.2 eV and 954.1 eV with the spin-orbital splitting of 19.9 eV and are attributed to Cu 2p_{3/2} and Cu 2p_{1/2}, respectively. The binding energy difference between these two peaks was found to be 19.9 eV which suggested the presence of the Cu²⁺ in the nanocatalyst [45]. Besides these, two satellite peaks were found at 943.3 and 963.2 eV due to Cu 2p_{3/2} and Cu 2p_{1/2}, further confirming the presence of CuO nanoparticles in the designed nanocatalyst. Most importantly, the peak appeared for C-P at 285.3 eV confirmed the presence of phosphate group on the GO surface.

Besides higher surface area, presence of different acidic groups (Lewis and Brönsted) on the nanocatalyst surface and their amount play an important role in the enhancement of its catalytic activity. In CuO/PGO, the presence of surface functional groups like alcohols and carboxylate groups on GO surface (as evidenced from XPS) provide Brönsted acidic sites [46]. In addition, GO surface has been functionalised with phosphate groups which is a well known Brönsted acidic group. On the other side, CuO also provides acidity as the copper site in CuO have great tendency to interact and co-ordinate with different functional group such as carbonyl (-CO), nitrile (-CN) and hydroxyl (-OH) and behaves as Lewis acid [47]. The Lewis acidity of Cu²⁺ is originated due to the acquirement of a stable and completely filled d-subshell on receiving an electron [48]. Therefore, in CuO/PGO nanocatalyst the

overall acidity originates from two types of acidic sites, i.e, Brönsted acidic sites from GO and phosphate group, and Lewis acidic sites from CuO nanoparticles.

To experimentally confirm the presence of such acidic sites in our nanocatalyst, NH_3 -TPD analysis was carried out. Fig. 5 (a) shows the NH_3 -TPD analysis of PGO and CuO/PGO nanocatalyst. *In NH_3 -TPD technique, basic NH_3 molecules adsorb on the catalyst surface and the acid groups are quantified by the amount of NH_3 molecules desorbed at different temperature. As this technique involves the adsorption and desorption of gas molecules with respect to temperature, total surface acidic density can be calculated by determining the amount of ammonia desorbed in milimole/gram on the surface of the catalyst. Based on this calculation, the total acidic sites present catalyst were found to be 0.59 mmol g^{-1} for CuO/PGO and 0.65 mmol g^{-1} for PGO (table S1). Normally, strong acidic sites are assigned for those peaks which appear above 400°C where as medium and weak acid sites for peaks around $200\text{--}400^\circ\text{C}$ and below 200°C , respectively [49]. Based on these observations, acidic site of 0.45 mmol g^{-1} can be assigned to strong acid sites and 0.14 mmol g^{-1} to medium acidic sites. However, there is no desorption peak found in weak acidic sites in the TPD profile. It is worth to mention here that *three peaks seen around 300°C in the NH_3 -TPD profile of CuO/PGO can be attributed to the desorption of chemisorbed NH_3 molecules from the catalyst surface due to the acidic nature of Cu^{2+} in the nanocatalyst. The possibility of these peaks due to acetate ions can be dismissed as the hydrolysis in water and isopropanol solvent followed by continuous washing led to the removal of these species as evidenced from FTIR studies and other reported literatures [50].* From the above result it can be inferred that our catalyst (CuO/PGO) had both Lewis as well as Brönsted acidic sites on its surface which play an important role in its catalytic activity for the synthesis of 3-Anilino-1, 3-diphenyl-1-propanone as discussed in more details in the catalytic study section. In addition, the combination of Brönsted acidic*

sites on GO and PGO and the Lewis acidic sites of CuO nanoparticles could also show possible synergistic effect in the nanocatalyst resulting in the higher activity [51].

To further validate the above results of NH₃-TPD analysis, pyridine-IR study was done (Fig. 5 (b)). In this study, the IR spectra of before and after adsorption of pyridine on *CuO/PGO* surface were recorded. From the figure three distinct peaks at 1541, 1489, and 1437 cm⁻¹ can be observed which were also seen in the IR spectra of PGO (Fig. 1 (b)). Additionally, two new peaks can be seen at 1469, and 1447 cm⁻¹ which are mainly due to the development of Lewis acidic sites on the catalytic surface. Among the observed peaks, the intense peak present at 1541 cm⁻¹ can be attributed to Brönsted acidic sites. This peak is mainly due to the the formation pyridinium ion resulting from the interaction of pyridine with Brönsted acidic sites [52]. A low intense peaks appeared nearly at 1437, 1447 and 1469 cm⁻¹ are due to the presence of Lewis acidic site [53]. *As discussed before, the source of these acidic sites are from GO, phosphate groups and CuO nanoparticles.*

3.2. Catalytic activity

After the successful synthesis and characterization of *CuO/PGO*, its catalytic activity was then investigated towards the synthesis of 3-anilino-1,3-diphenyl-1-propanone via one pot three component Mannich reaction of benzaldehyde, aniline and acetophenone (scheme 2). Design of a sustainable, cost-effective, environment friendly and green reaction pathway is the need of the hour for any organic transformation reaction. Ultrasonic route is found to be one such suitable pathway owing to its advantages like reduced energy consumption, easy reaction condition and short reaction time. In this regard, we had initially focused our investigation to establish a facile method for the synthesis of the desired product. The initial experiments were carried out with different catalysts under different synthetic conditions (table 2). It can be seen that trace amount of desire product was obtained in all the reaction conditions when there was no catalyst (entry 1, table 2) indicating the necessity of catalyst to

carry out the reaction. However, when the reaction was carried out in presence of catalysts like GO, PGO, Cu nanoparticles, CuO nanoparticle and *CuO/PGO*, higher yield of product was obtained (entry 3-8, table 2). *The equations used for calculation of product yield is given below [54].*

$$\text{Yield} = (m_{ap} / m_{tp}) \times 100 \dots\dots\dots (1)$$

Where m_{ap} is the actual mass of product and m_{tp} is the theoretical maximum mass of product.

Among these, the presence of *CuO/PGO* nanocatalyst resulted in a higher product yield (59% - 95%) in less reaction time (10-20 min) using all the available synthetic methods. Further, by comparing the efficiency of different synthetic routes such as grindstone, ultrasonic assisted, microwave and traditional stirring methods, it was found that ultrasonic assisted synthesis of 3-anilino-1,3-diphenyl-1-propanone led to the highest product yield (93%) in a reaction time of 15 min (entry 8, table 2) *demonstarating the effective role of ultrasonic process. Normally, the ultrasonic assisted reactions involve the interaction of ultrasonic radiation having a frequency above 20 kHz with the organic substrates. During this interaction process, transient cavities containing air or the vapours of liquid are formed which collapse vigorously after a few cycles of ultrasound. This process leads to enhancement of local temperatures and pressures inside the cavitating bubbles and at their interfaces. Therefore, these are known as the hot spots having higher temperature and pressure [55]. Overall, in this process the mechanical energy of mass flow is converted to kinetic energy of random molecular translation and rotation [56]. This above process helps in the breaking of chemical bonds while using ultrasonication route resulting in the generation of high product yield in shorter period of time. We have also carried out the reaction for a prolonged time (45-60 min) and found that maximum yield of 95% can be achieved within 15 min. When the reaction was continued for 60 min, the product yield was not changed significantly (91%). We have*

also calculated the TOF for all catalysts and the results are presented in table 3. *The equation used for calculation of TOF is given below [57].*

$$TOF = N_p / N_a \times Time (h) \dots\dots\dots (2)$$

Where N_p is the moles of substrate converted to product and N_a is the mole of acidic sites calculated from NH_3 -TPD.

Later on, to evaluate the effect of various reaction parameters on the product yield, the effect of solvents and instrumental frequency were investigated. The instrumental frequency was varied (45kHz and 65kHz) to know the optimized power of the ultrasonic irradiation. The product yield was found to be more (95%) in case of 65kHz frequency within same reaction time (15 min) as compared to instrument frequency (45kHz). The reaction was also carried out in both presence and absence of solvent under ultrasonic assisted method. Table 4 presents the obtained catalytic results. A higher product yield (95%) was found in solventless condition using ultrasonic assisted method with less time for the completion of the reaction (entry 5, table 4). This methodology is advantageous as many problems associated with the using solvents such as complex work-up procedure, safety, cost and environmental concern can be avoided by using solventless condition.

To further study the effect of CuO loading on *CuO/PGO*, the catalytic experiments were carried out (entries 1-4, Table S2) by varying the metal oxide loading from 5 to 20 wt%. The results showed that the product yield increased with the increase in CuO loading up to 10 wt% on the PGO catalyst. After that no significant change in product yield was observed with increase in metal oxide loading (entry 3-4, Table S1). Hence, 10 wt % *CuO/PGO* was considered as the optimized catalyst for the catalytic process. Further, to know the optimized and suitable amount of catalyst to be taken for high product yield, the catalyst amount was varied from 10 mg to 50 mg (Fig. 6). The product yield was found to be increased

linearly with increase in the amount of the catalyst up to 30 mg after which no significant change in the yield was obtained. *We have also varied the ratio of starting materials and carried out the reaction in similar condition and found that 1 milimole each of starting materials with a ratio of (1:1:1) results in high yield of product in the reaction.*

In order to investigate the efficiency and performance of our *CuO/PGO* catalyst using the optimized reaction conditions obtained from the above experiments, a wide range of substituted β -amino carbonyl compounds were synthesized (Table 5). We have varied the substituents in the aromatic aldehyde and aniline to check its effects on product yield and it was found that aromatic aldehydes with electron withdrawing groups led to a higher product yield in less time as compared to electron-donating substituents. Further, we have calculated the turn over frequency (TOF) of the nanocatalyst based of the total acidic sites for all derivatives (table 5). It can be observed from the table that high TOF value was obtained in all the cases which is quite useful for real time industrial applications. *The resulting products were analyzed well and confirmed by ^1H and ^{13}C NMR spectroscopy by comparing previously reported data.*

Another factor which affect the catalytic activity and product yield during a catalytic reaction is the synergistic effect of individual active sites present on the catalyst such as -COOH, -OH, phosphate group and CuO nanoparticle on *CuO/PGO*. To validate this characteristic effect a control experiment was carried out by protecting the hydroxyl and carboxylic groups with methoxytrimethylsilane (MTS) [58]. Initially, the catalyst was allowed to react with MTS for a particular time and then used as catalyst for the reaction. After the reaction, the product yield was found to be 45% which was less than that of fresh unreacted catalyst. This product yield of 45% mainly originated due to the presence of CuO nanoparticles which was very less as compared to unreacted *CuO/PGO* nanocatalyst. Besides, a physical mixture of PGO and CuO nanoparticles resulted in a product yield of 65% (entry 6, Table 2) which is

lower than that of CuO decorated PGO. These results confirmed the presence of synergistic effects between the individual component. Such synergistic effect would result in the significant adsorption of reactant molecules on *CuO/PGO* surface resulting in the enhancement of its catalytic activity. Existence of similar type of synergistic effects have been reported in previous literatures [59].

From all the results as discussed above, it can be concluded that the presence of acidic sites (Lewis and Brönsted), the synergistic effect among the individual component and higher surface area of *CuO/PGO* surface play an important role in its overall catalytic activity. Moreover, use of ultrasonic irradiation during the synthesis of β -amino carbonyl compounds stimulated the initiation of the reaction. A plausible mechanism can be elucidated considering all the above results and is presented in scheme 3. The acidic nature (both Brönsted and Lewis) of the catalyst and efficient chemical adsorption of reactant molecules on the catalyst surface initiate the interaction of acidic groups with aldehyde (IA) and amine substrates under ultrasonic irradiation. Due to this interaction, the carbonyl group was protonated and activated (mostly by the Brönsted acidic sites present on *CuO/PGO*). At the same time the aniline molecule (IB) also became activated by the Lewis acidic site (Cu^{2+}) [60]. Then the nucleophilic attack on activated aldehyde took place to form an iminium intermediate (II) via dehydration. The intermediate was stabilised by both the acidic sites thorough intermolecular bonding with -OH and -NH groups which further increased its electrophilicity. The intermediate then undergo nucleophilic attack by the activated acetophenone (generated by the interaction of active acidic sites of the *CuO/PGO* catalyst) to form the desired product. At the same time CuO nanoparticles binds properly with the organic substrates lowering the energy barrier required for all the intermediate steps [61]. Overall, the presence of both Cu^{2+} and phosphate groups help in the activation, stabilisation and formation of β -amino carbonyl compound. In addition, the efficient production of the desired product was influenced by cavitation induced by ultrasonic irradiations. Generation of huge amount of heat

energy and local pressure during the growth and collapse of microbubbles help in the efficient synthesis of β -amino carbonyl compounds. Mainly, during the formation of the intermediate (II), the dehydration process was favored by both ultrasonic irradiation as well as the acid groups present on the catalyst. Similar reaction mechanism for the synthesis of β -amino carbonyl compounds has been reported previously [62].

Recyclability and stability are the most important and essential characteristics of an efficient and useful catalyst. The optimized conditions were used to investigate the reusability of *CuO/PGO* catalyst. The catalyst was recovered after the completion of the reaction. It was washed properly with ethyl acetate to remove the organic parts and dried under vacuum at 80 °C for 3 h and reused six times with minimal loss of catalytic activity (Fig. 7). With the use of fresh sample, the product yield was found to be 95% which later became 82% after 6th catalytic run. These results suggest higher reusability of our nanocatalyst. The reused catalyst was further characterized by powder XRD and FTIR analysis. The similar pattern in XRD spectra and similar peaks in the FTIR spectra confirm the stability of the catalyst (Fig. S2). The strong bonding of individual active sites in the nanocatalyst makes it more active and reusable with minimal leaching of active sites like phosphate and CuO nanoparticles during the reaction. To confirm this, hot filtration test was carried out [63]. Briefly, benzaldehyde (1 mmol), aniline (1 mmol) and acetophenone (1 mmol) were taken in a round bottom flask and 0.015 gm of catalyst (*CuO/PGO*) was added and the reaction was put in sonication at a frequency of 65KHz for 7 min (Fig. 8). After that the catalyst was separated in hot condition and the product yield was found to be 53%. After the filtration process, the filtrate was allowed to continue under sonication for further reaction under same conditions. After 15 min of sonication the product yield was found to be 55% indicating minimal change in product yield. This change in product yield is not significant which confirms that

CuO/PGO is the active candidate for this catalytic process and no leaching of active sites during the reaction had occurred.

Later on, the advantages, efficiency and superiority of our designed nanocatalyst was demonstrated by comparing with other traditionally reported catalysts and are shown in table 6. It was found from the comparison data that our catalyst is superior as it shows higher activity within very short period of time via a green ultrasonic method as compared to other available catalyst such as γ - $\text{Al}_2\text{O}_3/\text{CH}_3\text{SO}_3\text{H}$ [29], K_3PO_4 [64], Tin(II)chloride [65], $\text{Fe}_3\text{O}_4@\text{ZrO}_2/\text{SO}_4^{2-}$ [66], CaCl_2 [67] and nano- $\text{Fe}_3\text{O}_4@\text{PEG-SO}_3\text{H}$ [68].

4. Conclusions

In summary, a novel nanocatalyst (CuO/PGO) was successfully synthesized and characterized by decorating CuO nanoparticles on phosphate functionalized graphene oxide. The acidic nature of the synthesized catalyst was investigated by NH_3 -TPD and Pyridine IR techniques by which total acidity was found to be 0.59 mmol g^{-1} . Later on, CuO/PGO catalyst was utilized as efficient catalyst for the synthesis of β -amino carbonyl compounds via one-pot multi-component reaction under greener ultrasonic route. As compared to other reported systems, our catalyst showed a higher product yield (95%) in a shorter period of time (15 min). This higher activity can be attributed to the presence of acidic sites, higher surface area, ultrasonication method and synergistic effects between the individual components. The catalyst showed excellent recyclability up to six consecutive runs without significant loss of catalytic activity with minimal leaching. The current methodology shows that by decorating suitable nanoparticles on acidic GO surface, highly efficient, stable and reusable catalyst can be designed which will have practical importance in various organic transformations.

Acknowledgements

The authors are thankful to Ministry of Human Resource Development (MHRD), Govt. of India, for funding.

References

- [1] G. Busca, *Chem. Rev.*, 107 (2007) 5366-5410.
- [2] S. You, Q. Cai, M. Zeng, *Chem. Soc. Rev.*, 38 (2009) 2190–2201.
- [3] V.S. Chary, K.C. Rajanna, G. Krishnaiah, P. Srinivas, *Catal. Sci. Technol.*, 6 (2016) 1430–1434.
- [4] P. Losch, J.F. Kolb, A. Astafan, T.J. Daou, L. Pinard, P. Pale, B. Louis, *Green Chem.*, 18 (2016) 4714–4724.
- [5] A.F. Silva, A. Fernandes, M.M. Antunes, P. Neves, S.M. Rocha, M.F. Ribeiro, M. Pillinger, J. Ribeiro, C.M. Silva, A.A. Valente, *Fuel*, 209 (2017) 371–382.
- [6] K.R. Sabu, R. Sukumar, R. Rekha, M. Lalithambika, *Catal. Today*, 49 (1999) 321-326.
- [7] T. Schoetz, C.P.d. Leon, A. Bund, M. Ueda, *Electrochim. Acta*, 263 (2018) 176-183.
- [8] C.K. Shin, S.J. Kim, G.J. Kim, *Tetrahedron Lett.*, 45 (2004) 7429–7433.
- [9] F. Liu, J. Sun, L. Zhu, X. Meng, C. Qi, F.S. Xiao, *J. Mater. Chem.*, 22 (2012) 5495-5502.
- [10] Y.N. Yue, W.J. Meng, L. Liu, Q.L. Hu, H. Wang, J.X. Lu, *Electrochim. Acta*, 260 (2018) 606-613.
- [11] Y. Mo, X. Zhao, T. Yuan, B. He, *J Chem Technol Biotechnol*, 93 (2018) 1388–1393.
- [12] L.S.K. Achary, A. Kumar, B. Barik, P.S. Nayak, N. Tripathy, J.P. Kar, P. Dash, *Sens. Actuator B-Chem.*, 272 (2018) 100–109.
- [13] A. Kumar, L. Rout, L.S.K. Achary, S.K. Mohanty, P. Dash, *New J. Chem.*, 41 (2017) 10568-10583.
- [14] L.S.K. Achary, A. Kumar, L. Rout, S.V.S. Kunapuli, R.S. Dhaka, P. Dash, *Chem. Eng. J.*, 331 (2018) 300–310.
- [15] Y. Chen, Q.L. Zhu, N. Tsumori, Q. Xu, *J. Am. Chem. Soc.*, 137 (2015) 106–109.
- [16] H. Wu, H. Shi, Y. Wang, X. Jia, C. Tang, J. Zhang, S. Yang, *Carbon*, 69 (2014) 379 – 389.
- [17] X. Liu, J. Li, X. Wang, C. Chen, X. Wang, *J. Nucl. Mater.*, 466 (2015) 56-64.
- [18] N. Oger, Y.F. Lin, C. Labrugere, E.L. Grogne, F. Rataboul, F.X. Felpin, *Carbon* 96 (2016) 342-350.
- [19] H. Steininger, M. Schuster, K.D. Kreuer, A. Kaltbeitzel, B. Bingöl, W.H. Meyer, S. Schauff, G. Brunklaus, J. Maiera, H.W. Spiess, *Phys. Chem. Chem. Phys.*, 9 (2007) 1764-1773.
- [20] S. Sahoo, T. Joseph, S.B. Halligudi, *J. Mol. Catal. A: Chem.*, 244 (2006) 179–182.
- [21] M. Kidwai, D. Bhatnagar, N.K. Mishra, V. Bansal, *Catal. Commun.*, 9 (2008) 2547–2549.
- [22] M.M. Heravi, V.F. Vavsari, *Adv. Heterocycl. Chem.*, 114 (2015) 77-145.
- [23] P. Ravichandiran, B. Lai, Y. Gu, *Chem. Rec.*, 17 (2017) 142-183.
- [24] Y. Morita, T. Yamamoto, H. Nagai, Y. Shimizu, M. Kanai, *J. Am. Chem. Soc.*, 137 (2015) 7075–7078.
- [25] J.S. Ghomi, S. Zahedi, *Appl. Organometal. Chem.*, 29 (2015) 566–571.
- [26] C. Chandler, P. Galzerano, A. Michrowska, B. List, *Angew. Chem. Int. Ed.*, 48 (2009) 1978 –1980.
- [27] S. Iimura, D. Nobutou, K. Manabe, S. Kobayashi, *Chem. Commun.*, 0 (2003) 1644–1645.
- [28] N. Azizi, L. Torkiyan, M.R. Saidi, *Org. Lett.*, 8 (2006) 2079–2082.
- [29] H. Sharghi, M. Jokar, *Can. J. Chem.*, 88 (2009) 14-26.
- [30] H. Ghafari, B. Ghorbani, A. Rashidzadeh, M. Talebi, M. Roshani, *Appl Organometal Chem.*, 32 (2018) 1-14.
- [31] S.G. Hosseini, R. Abazari, *RSC Adv.*, 5 (2015) 96777–96784.
- [32] K.N. Kudin, B. Ozbas, H.C. Schniepp, R.K. Prudhomme, I.A. Aksay, *R. Car, Nano Lett.*, 8 (2008) 36–41.

- [33] J.B. Goods, S.A. Sydlik, J.J. Walish, T.M. Swager, *Adv. Mater.*, 26 (2014) 718–723.
- [34] J. Zhu, G. Zeng, F. Nie, X. Xu, S. Chen, Q. Han, X. Wang, *Nanoscale* 2(2010) 988–994.
- [35] S. Chakraborty, A. Nair, M. Paliwal, A. Dybowska, S.K. Misra, *J Nanopart Res*, 20 (2018) 331.
- [36] M. Cochez, M. Ferriol, J. Weber, P. Chaudron, N. Oget, J. Mieloszynski, *Polym. Degrad. Stabil.*, 70 (2000) 455–462.
- [37] C. Sarkar, S.K. Dolui, *RSC Adv.*, 5 (2015) 60763–60769.
- [38] Z.S. Hong, Y. Cao, J.F. Deng, *Mater. Lett.*, 52 (2002) 34–38.
- [39] P.C. Rath, J. Patra, D. Saikia, M. Mishra, J.K. Chang, H.M. Kao, *J. Mater. Chem. A*, 4 (2016) 14222–14233.
- [40] L. Yin, H. Wang, L. Li, H. Li, D. Chen, R. Zhang, *Appl. Surf. Sci.*, 476 (2019) 107–114.
- [41] M. Ranjani, Y. Sathishkumar, Y.S. Lee, D.J. Yoo, A.R. Kim, G.G. kumar, *RSC Adv.*, 5 (2015) 57804–57814.
- [42] M. Vinothkannan, A.R. Kim, G.G. kumar, D.J. Yoo, *RSC Adv.*, 8 (2018) 7494–7508.
- [43] T. K. Shruthi, M. S. Kumar, M. Arjunan, A. Pratap, N. Chandrasekaran, *RSC Adv.*, 5 (2015) 93423–93432.
- [44] N. Senthilkumar, K.J. Babu, G.G. kumar, A.R. Kim, D.J. Yoo, *Ind. Eng. Chem. Res.*, 53 (2014) 10347–10357.
- [45] G. Li, N.M. Dimitrijevic, L. Chen, T. Rajh, K.A. Gray, *J. Phys. Chem. C*, 112 (2008) 19040–19044.
- [46] D.R. Dreyer, H.P. Jia, C.W. Bielawski, *Angew. Chem.*, 122 (2010) 6965–6968.
- [47] G.R. Chaudhary, P. Bansal, N. Kaur, S.K. Mehta, *RSC Adv.*, 4 (2014) 49462–49470.
- [48] V.S. Darshane, S.P. Ghorpade, S.G. Dixit, *Appl. Catal. B*, 166 (1998) 135–142.
- [49] R. Weingarten, Y.T. Kim, G.A. Tompsett, A. Fernández, K.S. Han, E.W. Hagaman, W.C.C. Jr., J.A. Dumesic, G.W. Huber, *J. Catal.*, 304 (2013) 123–134.
- [50] A.M.A. Sabagh, F.Z. Yehia, A.M.F. Eissa, M.E. Moustafa, G. Eshaq, A.M. Rabie, A.E. ElMetwally, *Polym. Degrad. Stab.*, 110 (2014) 364–377.
- [51] A. Kumar, L. Rout, L.S.K. Achary, R.S. Dhaka, P. Dash, *Scientific Reports*, 7 (2017) 42975.
- [52] Y. Chu, Z. Yu, A. Zheng, H. Fang, H. Zhang, S.J. Huang, S.B. Liu, F. Deng, *J. Phys. Chem. C*, 115 (2011) 7660–7766.
- [53] F. Hemmann, I.A. Telleria, C. Jaeger, E. Kemnitz, *RSC Adv.*, 5 (2015) 89659–89668.
- [54] A.P. Dicks, *Current Opinion in Green and Sustainable Chemistry*, 13 (2018) 27–31.
- [55] G. Cravotto, P. Cintas, *Chem. Soc. Rev.*, 35 (2006) 180–196.
- [56] J. Ji, J. Wang, Y. Li, Y. Yu, Z. Xu, *Ultrasonics*, 44 (2006) e411–e414.
- [57] L. Li, T.I. Korányi, B.F. Sels, P.P. Pescarmona, *Green Chem.*, 14 (2012) 1611–1619.
- [58] J. Ji, G. Zhang, H. Chen, S. Wang, G. Zhang, F. Zhang, X. Fan, *Chem. Sci.*, 2 (2011) 484–487.
- [59] Q. Huang, L. Zhou, X. Jiang, Y. Zhou, H. Fan, W. Lang, *ACS Appl. Mater. Interfaces*, 6 (2014) 13502–13509.
- [60] G.V. Botteselle, M. Godoi, F.Z. Galetto, L. Bettanin, D. Singh, O.E.D. Rodrigues, A.L. Braga, *J. Mol. Catal. A: Chem.*, 365 (2012) 186–193.
- [61] S.G. Babu, P.A. Priyadarsini, R. Karvembu, *Appl. Catal. A*, 392 (2011) 218–224.
- [62] S. Saikia, P. Gogoi, A.K. Dutta, P. Sarma, R. Borah, *Journal of Molecular Catalysis A: Chemical*, 416 (2016) 63–72.
- [63] P. Puthiaraj, K. Pitchumani, *Green Chem.*, 16 (2014) 4223–4233.
- [64] B. Movassagh, S. Khosousi, *Monatsh. Chem.*, 143 (2012) 1503–1506.
- [65] M. Wang, Z.G. Song, X. Wan, S. Zhao, *Monatsh. Chem.*, 140 (2009) 1205–1208.
- [66] H. Ghafari, B. Ghorbani, A. Rashidizadeh, M. Talebi, M. Roshani, *Appl Organometal Chem.*, 32 (2018) 4147.

- [67] P. Kulkarni, B. Totawar, P.K. Zubaidha, *Monatsh. Chem.*, 143 (2012) 625–629.
- [68] A. Maleki, P. Zand, Z. Mohseni, R.F. Haji, *Nano-Structures & Nano-Objects* 16 (2018) 31-37.

Journal Pre-proof

Figure Captions

Fig. 1. (a) XRD pattern of GO, PGO and PGO-CuO and (b) FTIR spectra of GO, PGO and PGO-CuO nanocomposite.

Fig. 2 HRTEM image of (a, b, d) PGO-CuO and (c) Histogram plot for particle size (e) SAED image of PGO-CuO nanocomposite.

Fig. 3 N₂ adsorption-desorption study of GO and PGO-CuO nanocomposite.

Fig. 4. XPS Survey spectra of (a) PGO-CuO (b) C1s XPS spectra of GO, (c) C1s XPS spectra of PGO-CuO, (d) P 2p XPS spectra of PGO-CuO and (e) Cu2p XPS spectra of PGO-CuO nanocomposite.

Fig. 5 (a) Ammonia TPD profile of PGO and PGO-CuO and (b) Pyridine adsorbed IR spectra of PGO and PGO-CuO nanocomposite.

Fig. 6 Influence of the PGO-CuO amount on reaction yield at a constant time.

Fig. 7 Reusability study of PGO-CuO catalyst.

Fig. 8 Leaching study of PGO-CuO catalyst.

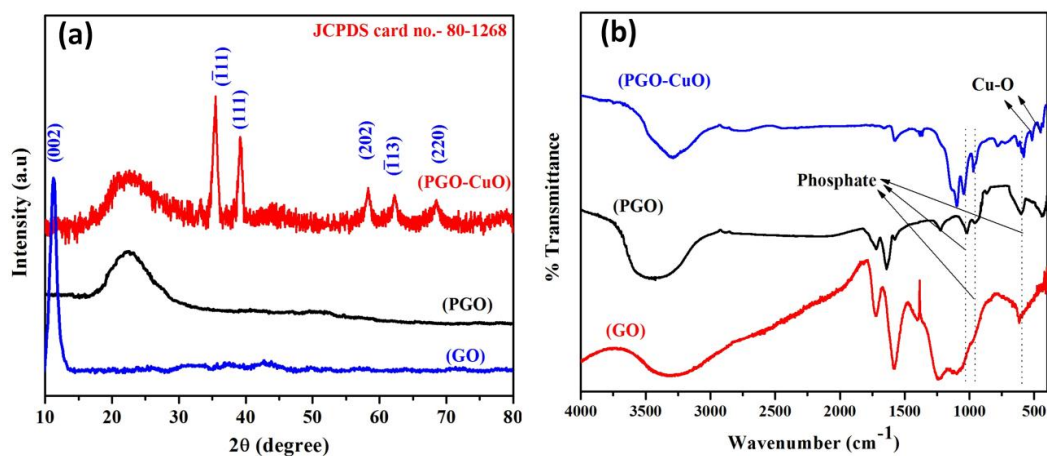


Fig.1. (a) XRD pattern of GO, PGO and PGO-CuO and (b) FTIR spectra of GO, PGO and PGO-CuO nanocomposite.

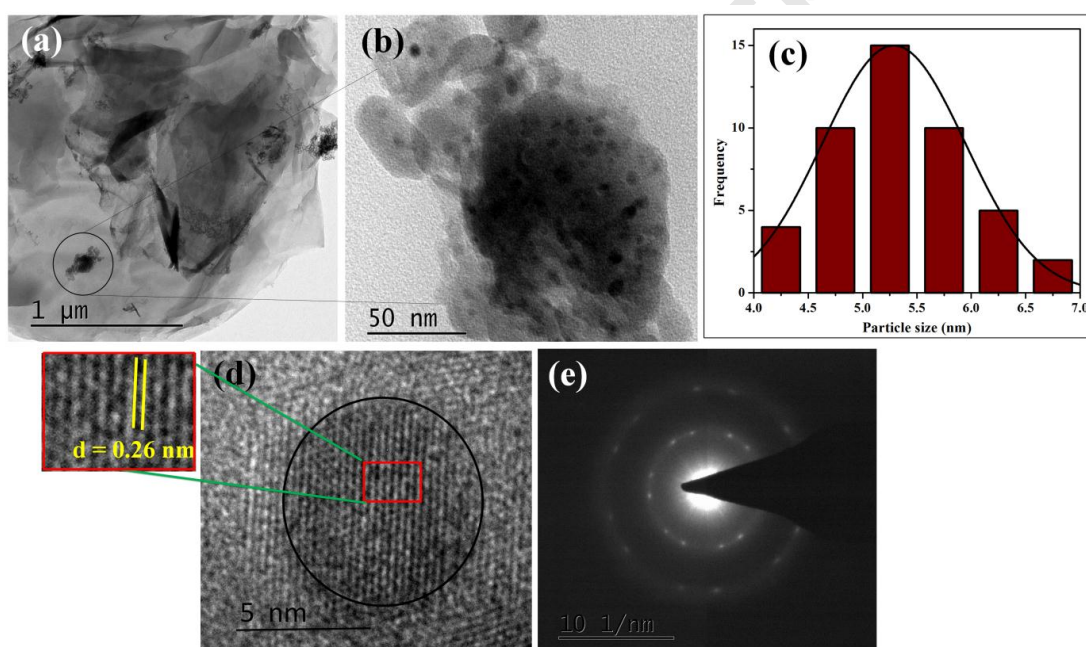


Fig. 2 HRTEM image of (a, b, d) PGO-CuO and (c) Histogram plot for particle size (e) SAED image of PGO-CuO nanocomposite.

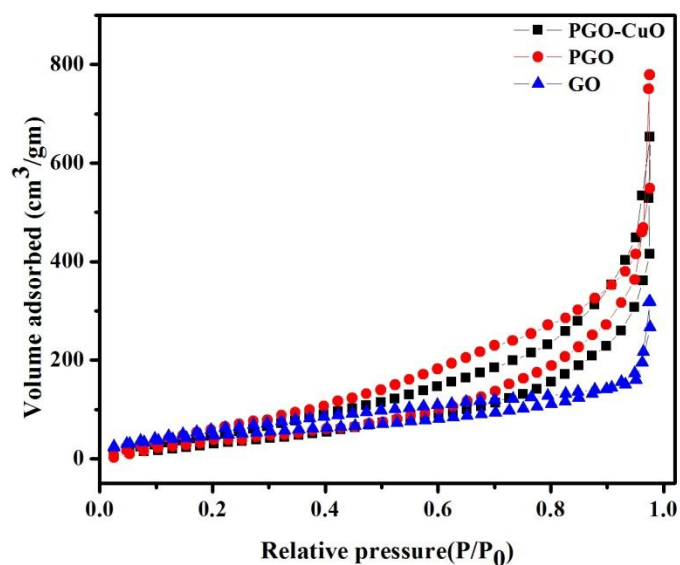


Fig.3 N₂ adsorption-desorption study of GO and PGO-CuO nanocomposite.

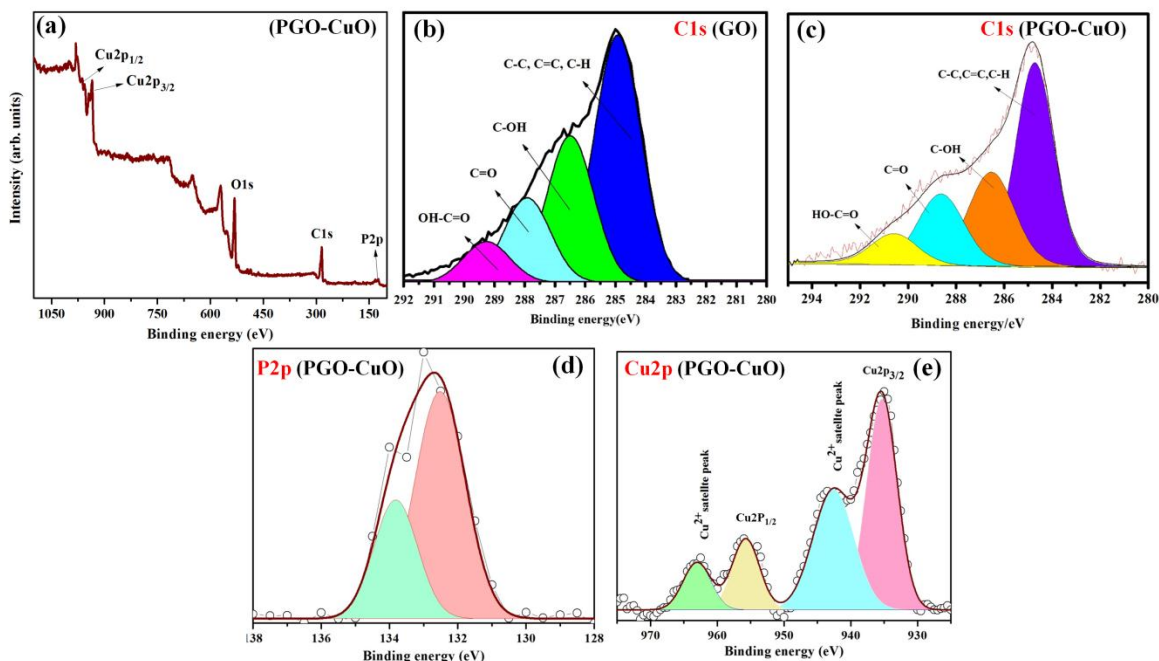


Fig.4. XPS Survey spectra of (a) PGO-CuO (b) C1s XPS spectra of GO, (c) C1s XPS spectra of PGO-CuO, (d) P 2p XPS spectra of PGO-CuO and (e) Cu2p XPS spectra of PGO-CuO nanocomposite.

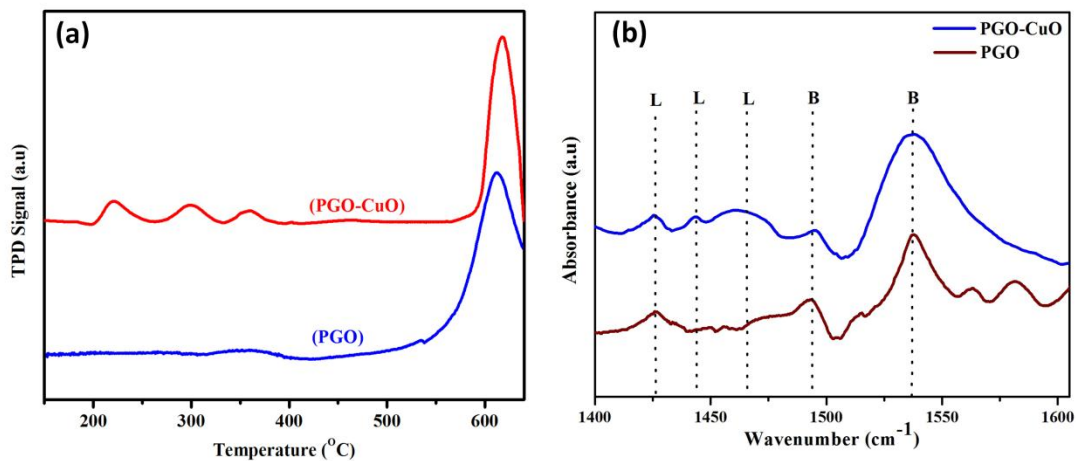


Fig . 5 (a) Ammonia TPD profile of PGO and PGO-CuO and (b) Pyridine adsorbed IR spectra of PGO and PGO-CuO nanocomposite.

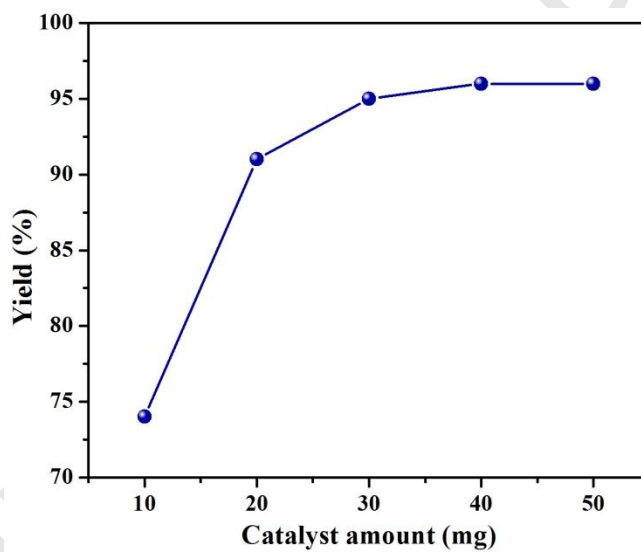


Fig. 6 Influence of the PGO-CuO amount on reaction yield at a constant time.

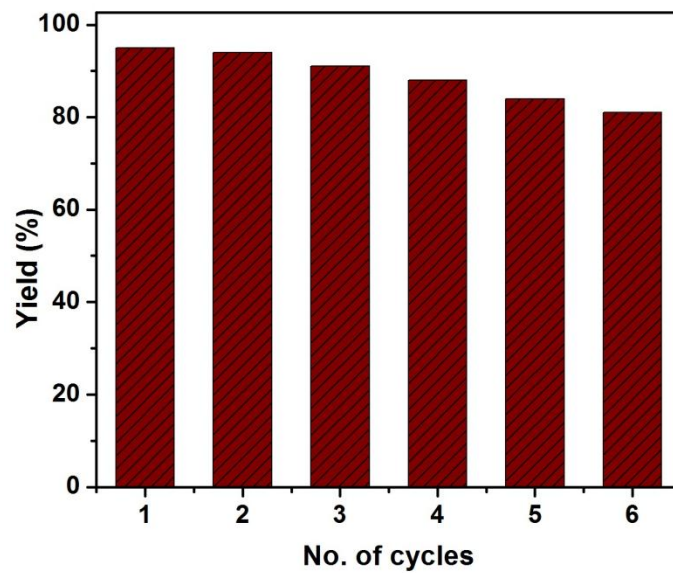


Fig. 7 Reusability study of PGO-CuO catalyst.

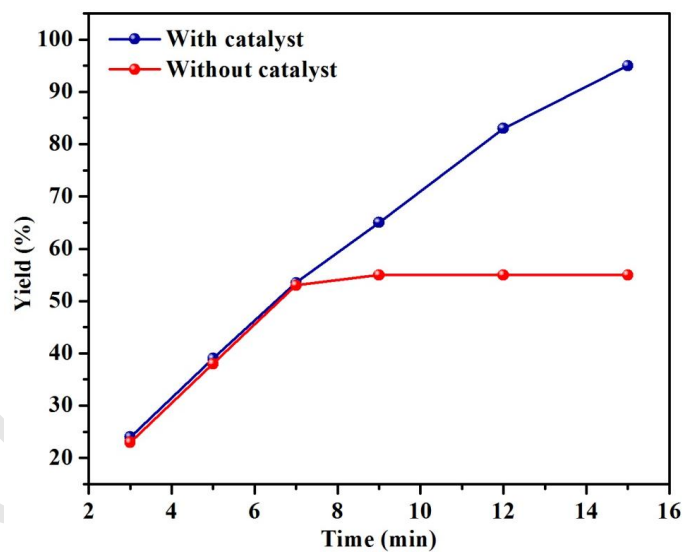


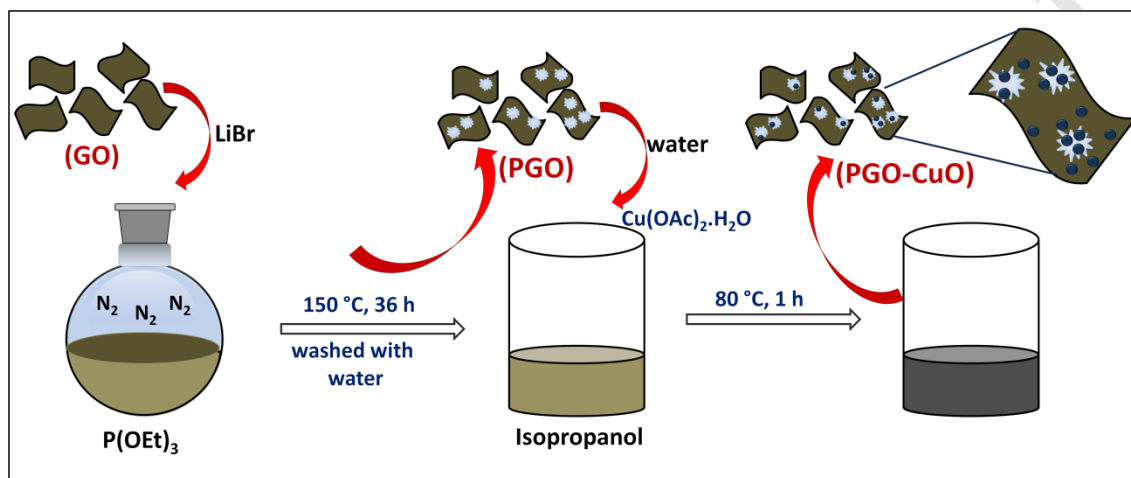
Fig. 8 Leaching study of PGO-CuO catalyst.

Scheme Captions

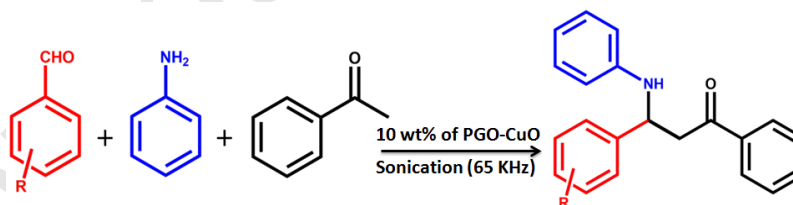
Scheme 1: Schematic diagram for the synthesis of PGO-CuO catalyst.

Scheme 2: A model reaction for the synthesis of 3-Anilino-1, 3-diphenyl-1-propanone.

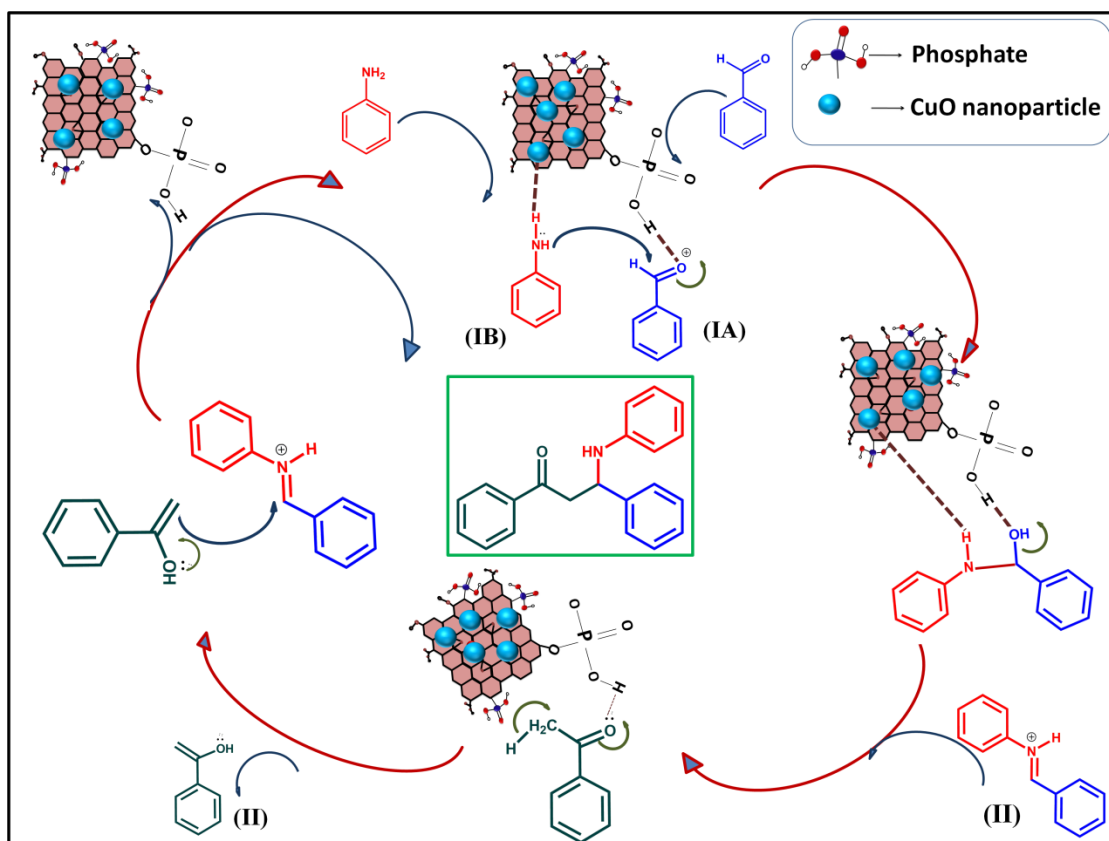
Scheme 3: Plausible reaction mechanism for the synthesis of 3-Anilino-1, 3-diphenyl-1-propanone.



Scheme 1. Schematic diagram for the synthesis of PGO-CuO catalyst.



Scheme 2: A model reaction for the synthesis of 3-Anilino-1,3-diphenyl-1-propanone.



Scheme 3: Plausible reaction mechanism for the synthesis of 3-Anilino-1, 3-diphenyl-1-propanone.

Table captions

Table 1. Surface area analysis of GO, PGO and PGO-CuO.

Sample	BET surface area (m ² g ⁻¹)
GO	154
PGO	179
PGO-CuO	162

Table 2. Synthesis of 3-anilino-1, 3-diphenyl-1-propanone by different catalyst and different synthetic methods under solventless conditions.

Entry	Catalyst	Time (min)/Yield (%)			
		US (r.t.)	Grindstone (r.t.)	Traditional stirring (r.t.)	MW (150W)
1	-----	15/trace	15/trace	20/trace	10/trace
2	graphite	15/7	15/trace	20/15	10/17
3	GO	15/10	15/8	20/20	10/11
4	PGO	15/46	15/23	20/42	10/39
5	CuO	15/26	15/19	20/32	10/32
6	PGO+CuO	15/64	15/38	20/53	10/45
	physical mixture				
7	Cu	15/21	15/15	20/19	10/28
	nanoparticle				
8	PGO-CuO	15/93	15/59	20/89	10/75

Reaction conditions: benzaldehyde (1 mmol), aniline (1 mmol) and acetophenone (1 mmol). isolated yield. US (45W).

Table 3. Catalytic activity of different catalyst on the synthesis 3-Anilino-1,3-diphenyl-1-propanone.

Entry	Catalyst	Yield (%)	Based on number of acidic sites	Based on number of metal sites
			TOF ^a	TOF ^b
1	No catalyst	Trace	--	--
1	PGO	46	97	--
2	Cu nanoparticle	21	--	42
3	CuO	26	--	52
4	CuO/PGO	95	223	190

Reaction conditions: benzaldehyde (1 mmol), aniline (1 mmol) and acetophenone (1 mmol), 0.02 mmol metal nanocomposite (2 mol % vs. substrate), time (15 min), isolated yield. Acidic site was calculated from NH₃-TPD analysis.

^aTurn over frequency (TOF) = moles of substrate converted to product per mole of active sites (based on total acidic sites) per hour

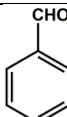
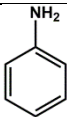
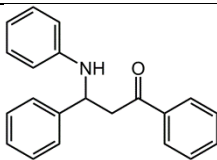
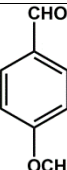
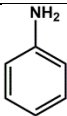
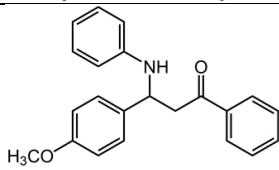
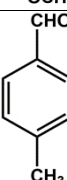
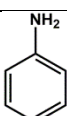
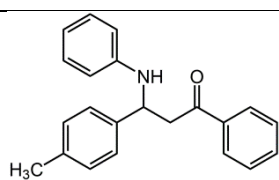
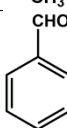
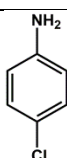
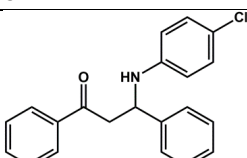
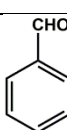
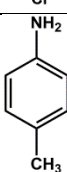
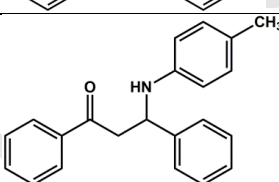
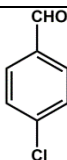
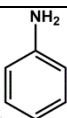
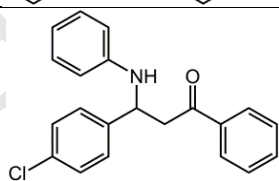
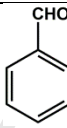
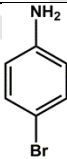
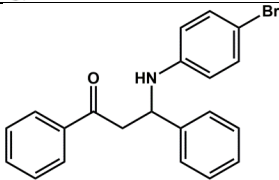
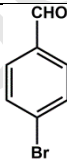
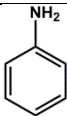
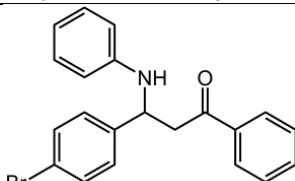
^bTurn over frequency (TOF) = moles of substrate converted to product per mole of metal catalyst per hour.

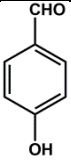
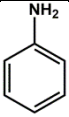
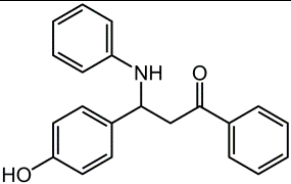
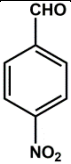
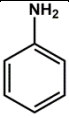
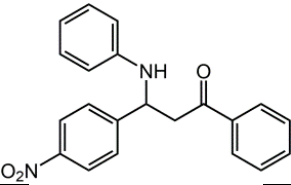
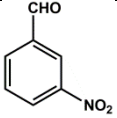
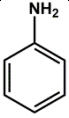
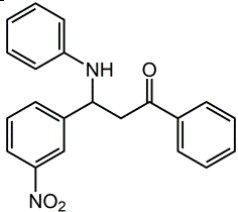
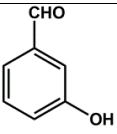
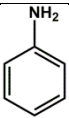
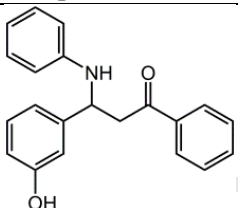
Table 4. Effect of solvent and ultrasonic power on the synthesis 3-anilino-1, 3-diphenyl-1-propanone.

Entry	Solvent	Power (kHz)	Time (min)	Yield (%)
1	Solventless	45	15	93
2	Solventless	65	15	95
3	Ethanol	65	15	81
4	Water	65	15	75
5	Solventless	65	15	95
6	DCM	65	15	53
7	Acetonitrile	65	15	68
8	DMSO	65	15	73
9	Hexane	65	15	20

Reaction conditions: benzaldehyde (1 mmol), aniline (1 mmol) and acetophenone (1 mmol), time (15 min). isolated yield.

Table 5. Synthesis of β -amino carbonyl derivatives catalyzed by PGO-CuO catalyst under traditional and ultrasonic methods.

S. no.	Benzaldehyde	Aniline	Product	Traditional method	Ultrasonic method	TOF ^a
				Time (min)/Yield (%)		
4a				20/89	15/95	223
4b				20/86	15/90	211
4c				20/85	15/91	214
4d				20/88	14/93	237
4e				20/83	15/91	214
4f				20/90	13/94	255
4g				20/85	15/92	216
4h				20/88	14/93	237

4i				20/84	15/89	209
4j				20/88	15/93	218
4k				20/87	15/90	211
4l				20/85	15/92	216

^aTurn over frequency (TOF) = moles of substrate converted to product per mole of acidic site (based on total acidic sites obtained from NH₃-TPD) per hour.

Table 6. Comparison of the catalytic activity of PGO-CuO with the reported catalysts for the synthesis of 3-anilino-1, 3-diphenyl-1-propanone.

Entry	Catalyst	Condition	Time (min)	Yield (%)	Ref.
1	γ -Al ₂ O ₃ /CH ₃ SO ₃ H	Solventless (r.t.)	60	92	29
2	K ₃ PO ₄	Ethanol (r.t.)	40	90	64
3	Tin(II)chloride	Ethanol (20 °C)	6 h	91	65
4	Fe ₃ O ₄ @ZrO ₂ /SO ₄ ²⁻	Solventless (60 °C)	30	96	66
5	CaCl ₂	Ethanol (60 °C)	120	72	67
6	Nano-Fe ₃ O ₄ @PEG-SO ₃ H	Ethanol (r.t.)	25	94	68
7	PGO-CuO	Solventless (r.t.)	15	95	Present work